PHYSICAL REVIEW C VOLUME 14, NUMBER 6 DECEMBER 1976

Isospin-mixed ^{18}F states seen via ^{14}N(α,α_1)^{14}N(2.31 MeV)†

L. C. Chen*
Department of Physics, University of Wisconsin, Madison, Wisconsin 53706
(Received 23 February 1976)

Extensive differential cross section measurements are reported for the isospin-forbidden reaction ^{14}N(α,α_1)^{14}N over the energy range $7.6 < E_\alpha < 16.9$ MeV at 11 to 16 angles. A partial wave analysis with a new method of removing ambiguities and parametrizing S matrix elements yields the level parameters of 151 isospin-mixed, natural-parity states in ^{18}F. These level parameters satisfactorily reproduce all the data. Many of these ^{18}F states correspond to those seen via ^{16}O(d,α_1)^{14}N. A number of levels have been identified as the analogs of $T=1$ states in ^{18}O. Correlations in $S_l(E_x)$ suggest intermediate structure and support Friedman's bridge state hypothesis.

[NUCLEAR REACTIONS ^{14}N(α,α_1), $E=7.6$–16.9 MeV; measured $\sigma(E,\theta)$: θ = 20–165°, ΔE = 20–30 keV. Deduced ^{18}F level parameters, S matrix analysis, new method excluding ambiguous solutions. Isospin mixing, deduced IAS.]

I. INTRODUCTION

The primary purpose of the present experiment was to use the isospin-forbidden reaction ^{14}N(α,α_1)^{14}N (2.31 MeV) as a tool to obtain spectroscopic information in a very complex region of the compound nucleus ^{18}F and to compare the results with the ^{16}O(d,α_1)^{14}N study of Jolivette.[1]

Two common properties make these reactions especially powerful and selective for the spectroscopic study of ^{18}F. First, they both violate isospin conservation because each incoming channel has a total isospin 0 while each outgoing channel has a total isospin 1. Therefore, these reactions can only go through those ^{18}F states which are mixtures of T=0 and T=1. Second, both reactions involve three 0^+ states and one 1^+ state. With this special combination of spins and parities, only the natural parity states in ^{18}F can be involved, but 0^+ states of ^{18}F are strictly forbidden.[2,3] Also the partial wave expansion of the differential cross section for this special combination of spins and parities is particularly simple.[3]

At the same excitation energy in ^{18}F more partial waves contribute to the ^{14}N(α,α_1)^{14}N reaction than to the ^{16}O(d,α_1)^{14}N reaction because the former has a lower centrifugal barrier in the incident channel. Therefore, ^{14}N(α,α_1)^{14}N is a better tool to study the high spin states of ^{18}F. We hoped to test whether the same ^{18}F states were important in these two reactions and to obtain better information about those high spin states which were barely detectable or even missing in the ^{16}O+d channel. In addition, we sought to identify in ^{18}F the T=1 states which are analogs of ^{18}O states.

Lane and Thomas[4] suggested that at higher excitation energies isospin conservation should first return for the low partial waves. This prediction was not verified in the ^{16}O+d channel,[1] and we wondered if the result would be the same in ^{14}N(α,α_1)^{14}N.

Jolivette[1] found correlations between levels of the same J^π such that the complex amplitudes of nearby levels often summed approximately to zero. This result Friedman[5] explained in terms of intermediate structure and bridge states. We hoped that a restudy of ^{14}N(α,α_1)^{14}N would provide more tests of this explanation.

To reach these goals, we needed precise and extensive ^{14}N(α,α_1)^{14}N data and very reliable analysis procedures. Most of the earlier measurements on ^{14}N(α,α_1)^{14}N by Tollefsrud and Jolivette[6] lacked simultaneous data at a sufficient number of angles to fix reliably the high partial waves. Also, the energy steps of 30 keV through the entire energy range were marginal for some of the narrower resonances.

In the present work the much thinner detectors now available enabled us to extend Tollefsrud's and Jolivette's data to lower energies (10.2 MeV > E_α > 7.67 MeV). This extension was important to overlap the ^{18}F excitation region where the ^{16}O(d,α_1)^{14}N results were most reliable. Then we remeasured the data for the energy region 10.2 < E_α < 16.81 MeV in smaller steps and at more angles. We also developed a new procedure[7] of removing ambiguities and parametrizing S-matrix elements in the partial wave analysis. This new procedure was important for the successful analysis of the data.

II. EXPERIMENTAL PROCEDURE

Alpha particles from our EN tandem Van de Graaff were used to bombard a gaseous nitrogen target in the differentially pumped scattering chamber described in Ref. 6. The target gas of research grade nitrogen (99.995% pure) entered the scattering chamber after first passing through a cold trap of dry ice and acetone mixture. No contamination was ever detected. The target gas pressure was about 10 Torr throughout the experiment. For a given pressure, the target thickness is still a function of detector slit geometry and laboratory angle. Our values varied from 8 to 15 keV at θ_{lab} = 20°, 3 to 6 keV at θ_{lab} = 95°, and 11 to 18 keV at θ_{lab} = 165°. The He^- ion source for injection into the tandem accelerator was similar to that described by Tollefsrud[8]. The He^- output was 1 - 4 μA, but only 100 - 400 nA doubly charged α particles after collimation to ±0.1° finally traversed the gas scattering chamber. The scattered alphas, after collimation by slits, were re-

corded by solid state detectors whose thickness (from 11 μm to 300 μm) optimized the signal from the alpha group of interest. Signals, after amplification, passed through analog to digital converters (ADCs) to an on-line buffered scope display and finally were recorded on magnetic tape for off-line data reduction. In general the detectors used were thin enough to let proton and deuteron peaks fall well below α_1. Since the α_1 group was well separated from other groups, the background corrections were rather simple. We found it sufficient to subtract the backgrounds by visual adjustment of the background lines using the cathode ray tube (CRT) and a light pen. This was done off-line on our DDP-124 computer.

Apart from statistical uncertainties the overall systematic errors add to <3%. In addition there are ~2% random errors. These uncertainties usually dominate when the cross sections are high. Statistical uncertainties when larger than the datum point size are shown on the cross section figures. See Ref. 9 for details of the error analysis.

Our measurements consist of excitation functions taken simultaneously at 11 to 16 angles and in E_α steps of 30 keV for $7.67 < E_\alpha < 8.46$ MeV and $9.13 < E_\alpha < 10.33$ MeV; 20 keV for $8.46 < E_\alpha < 9.13$ MeV and $E_\alpha > 10.33$ MeV. The lower energy limit resulted from our inability to separate the low energy inelastic α particles from protons and deuterons at backward angles. The measurements terminated at high energies because so many partial waves were important that analysis became difficult.

III. RESULTS

Figures 1 through 6 show the excitation functions measured in the reaction $^{14}N(\alpha,\alpha_1)^{14}N$. In all figures, the lower energy scale is the laboratory alpha beam energy and the upper energy scale is the ^{18}F excitation energy, both corrected for energy loss to the center of the target chamber. Data taken at fixed lab angles give energy dependent center of mass angles as indicated in the figures. The error bars correspond to statistical errors and are shown only when they exceed the datum point size. The solid curves are the differential cross sections calculated from our ^{18}F level parameters as discussed below.

At energies and angles where the present data overlap that of Tollefsrud and Jolivette[6] the agreement is generally within the combined uncertainties of the two experiments.

IV. ANALYSIS

In order to obtain complete and reliable information about the isospin-mixed ^{18}F states, we put great effort on the analysis of the $^{14}N(\alpha,\alpha_1)^{14}N$ data. Our goal was to find a set of level parameters in ^{18}F which can fully describe the data, that is, which can satisfactorily reproduce all the cross section measurements. To achieve this goal, we first expanded the angular distributions in partial waves and obtained the complete set of ambiguous solutions for the S-matrix elements. Next we removed the ambiguities by applying some unique properties among these solutions. The selected "physical" solution was then parametrized into coherent sums of Breit-Wigner resonances. In doing this, both the magnitudes and phases of the partial waves were considered. This procedure enabled the level parameters to reproduce

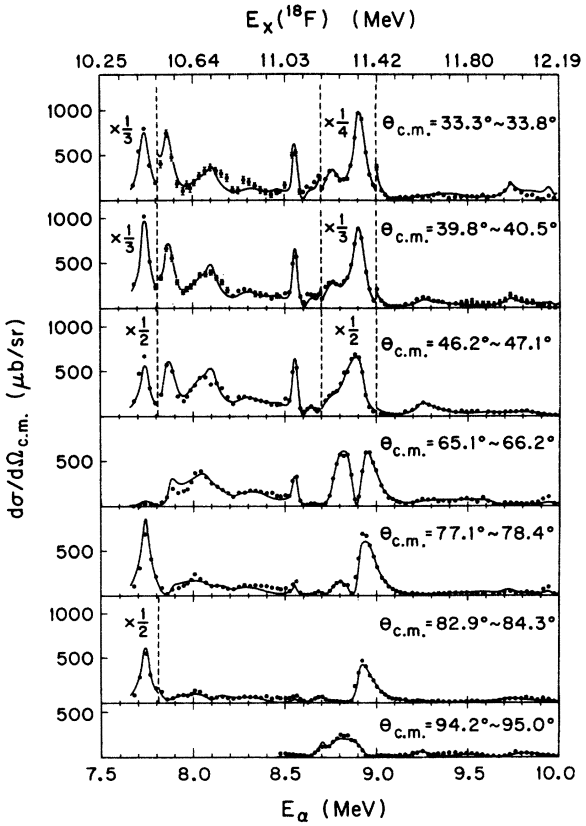

FIG. 1. $^{14}N(\alpha,\alpha_1)^{14}N$ differential cross sections. Both the E_α scale and the $E_x(^{18}F)$ scale have been corrected for energy loss to the center of the target chamber. The data were taken at fixed laboratory angles and the center of mass angles for the lowest and highest energy points on each plot are indicated. The error bars represent the uncertainties from counting statistics and background subtraction, and are shown whenever they are larger than the point size. The solid curves are the differential cross sections calculated from our ^{18}F level parameters in Table I.

satisfactorily the data. The detailed analysis procedure is reported in the author's thesis[9] and will be published separately. In the following, we will briefly describe each step and present the result.

Jolivette and Richards[3] showed that the differential cross section of any reaction with three 0^+ states and one 1^+ state can be expanded into partial waves according to the rather simple formula:

$$\frac{d\sigma}{d\Omega} = \frac{\lambda^2}{12} \left| \sum_{\ell=1}^{L} \frac{2\ell+1}{\sqrt{\ell(\ell+1)}} S_\ell \frac{dP_\ell(\cos\theta)}{d\theta} \right|^2, \quad (1)$$

where S_ℓ is the ℓ^{th} partial wave of the complex S-matrix element, $P_\ell(\cos\theta)$ is the ordinary Legendre polynomial of order ℓ, and L is the maximum ℓ value necessary to give satisfactory angular distribution fits.

At each energy, a nonlinear χ^2 fit with Eq. (1)

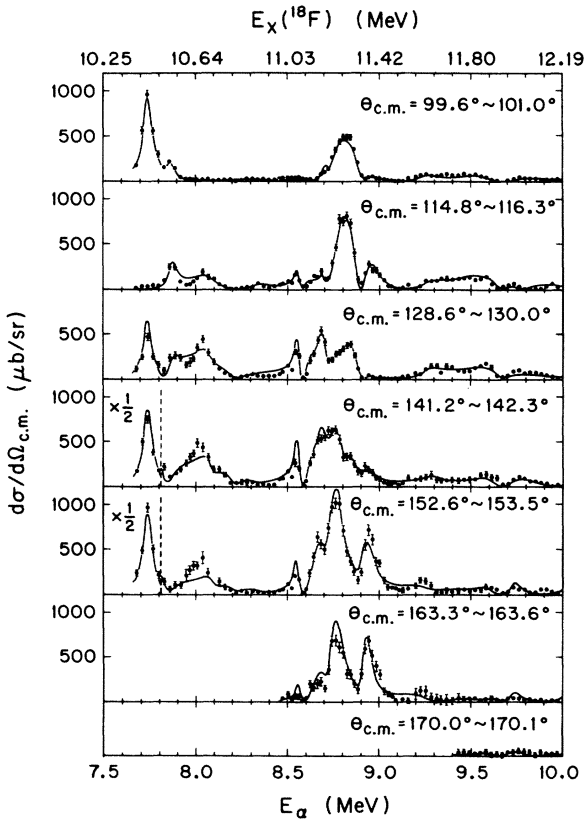

FIG. 2. The same as Fig. 1 but for different angles.

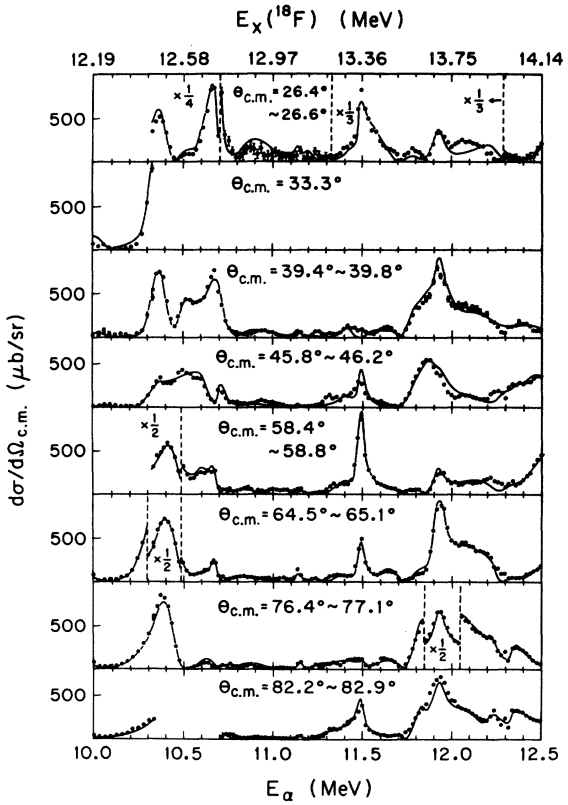

FIG. 3. The same as Fig. 1 but for different energies and angles.

was made to the angular distribution data. Figures 7 through 9 show samples of these fits and typical confidence levels (C.L.) of the fits ($0.1 < \text{C.L.} < 0.9$ is acceptable). Because of the squaring in Eq. (1), there are 2^L sets of different S-matrix elements that give identical angular distribution fits. Among these solutions, 2^{L-2} sets are different in magnitude.[10] Gersten's method[11] was used in obtaining all ambiguous solutions. In this method, once a set of S_ℓ is obtained from the best fit of the angular distribution with arbitrary starting values, all other solutions of S_ℓ can be generated by first calculating the complex zeros of the scattering amplitude, then complex conjugating different sets of them.

The most difficult part in the analysis was to remove the ambiguities. Jolivette[1,10] did this by first sorting the degenerate solutions into consistent energy-dependent sets and then selecting the simplest solution as the "physical" solution. However, for our $^{14}N(\alpha,\alpha_1)^{14}N$ analysis we found some problems and difficulties particularly in staying with the same solution as the energy varied. To overcome the difficulties, I developed a new and simpler method[7,9] of selecting the physical solution based on the fact that $|S_L|$ and $|S_L|\cos(\phi_{L-1}-\phi_L)$ are unique[3] for all ambiguous solutions, where $S_\ell = |S_\ell|\, e^{i\phi_\ell}$ for ℓ=1 to L.

Like Jolivette[10] our basic assumption is that the physical solution is the one requiring the fewest ^{18}F states to account for the cross section data as a function of energy. Consider first the partial wave of highest ℓ since the extracted $|S_L|$ is unique.[3] If one parametrizes the $|S_L|$ over an extended energy range with the smallest possible coherent sum of Breit-Wigner resonances,

$$S_\ell = \sum_\lambda \frac{a_{\ell\lambda} + ib_{\ell\lambda}}{(E-E_{\ell\lambda})+i(\Gamma_{\ell\lambda})/2} \qquad (2)$$

then the resulting level parameters for S_L also suffice to fix the relative phase ϕ_L as a function of energy. But since the extracted $|S_{L-1}|\cos(\phi_{L-1}-\phi_L)$ is also unique,[3] one can next use Eq. (2) for fitting this second unique function with the fewest levels. Finally one varies simultaneously the level parameters for both S_L and S_{L-1} until one obtains the minimum total chi squares for the two unique quantities. We then have reliable level parameters from which we can calculate $|S_{L-1}|$ as a function of energy. These values of $|S_{L-1}|$ should at each energy correspond to one of the earlier ambiguous set of $|S_{L-1}|$. If several of the ambiguous $|S_{L-1}|$ lie close to the calculated value, usually an examination of $|S_{L-2}|$, $|S_{L-3}|$ etc. will tell us which solution has the simplest structure. If this examination is unsuccessful, then the same technique applied to S_{L-1} can be extended to S_{L-2} for those $|S_{L-1}|$ which have nearly the same value. In these cases $|S_{L-2}|\cos(\phi_{L-2}-\phi_L)$ becomes unique.

The new method selected an unambiguous solution without much difficulty. Figures 10 through 12 show the magnitudes of the resultant S-matrix elements for the entire energy region. The uncertainties shown for each partial wave are average values obtained from the angular distribution fits.

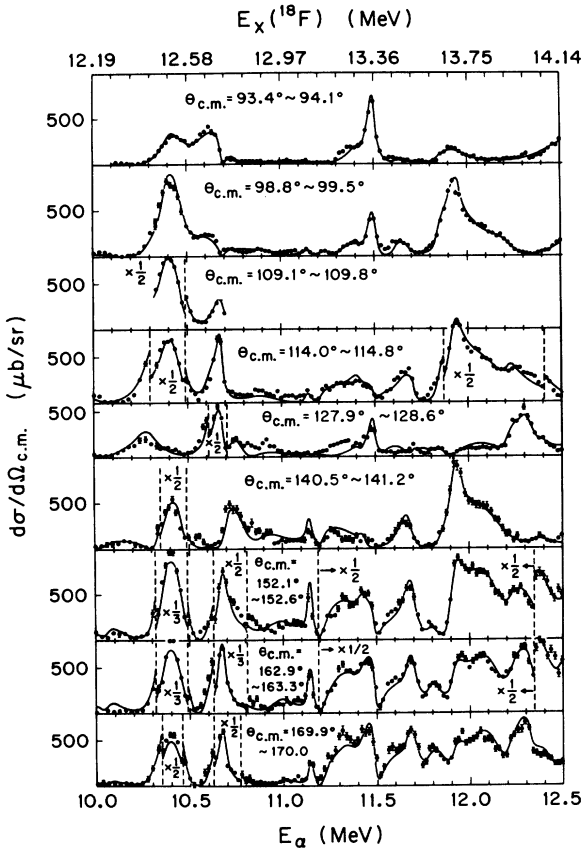

FIG. 4. The same as Fig. 1 but for different energies and angles.

The lower partial waves have larger uncertainties because they are less sensitive to the angular distributions.

Tollefsrud and Jolivette[6] (TJ) also extracted the $|S_\ell|$'s for $10.3 < E_\alpha < 12.7$ (see Fig. 14 of Ref. 6) but did not fit the $|S_\ell|$'s to Breit Wigner resonances. Our $|S_\ell|$'s are in fair agreement for $\ell \geq 4$ but show increasingly less correspondence for $\ell < 4$. This result is not surprising since TJ's analysis antedated procedures for eliminating ambiguous solutions and hence would uniquely fix only $|S_L|$. The strong resonances for $\ell < L$ still appear in TJ's extracted $|S_\ell|$ but sometimes shifted in energy perhaps because of their choice of the wrong solution set. The $|S_\ell|$ between the resonances show no correspondence to the present solution.

The solid curves shown in Fig. 10-12 result from the parametrization of the selected S-matrix elements in terms of coherent Breit-Wigner resonances, Eq. (2). The corresponding level parameters are in Table I. The procedure, for each partial wave, involved simultaneous fits of both $|S_\ell|$ and $|S_\ell|\cos(\phi_\ell-\phi_L)$ with the least number of levels necessary to give satisfactory chi squares. Because both the magnitudes and the phases of each partial wave have been included in the fitting, the resulting level parameters not only give the correct $|S_\ell|$ but also the correct ϕ_ℓ for each ℓ and hence should reproduce all the differential cross sections. Indeed, we found that the level parameters so obtained did reproduce all the differential cross section data satisfactorily as shown by the solid curves in Figs. 1-6. Absolute uncertainties in the level parameters are difficult to estimate. However, the uncertainties are in general higher for states of lower spins, weaker intensities or larger widths.

As a test of the reliability of our analysis, we did apply our parametrization procedure to a synthetic problem where we knew the physical solution. For the unphysical (ambiguous) solutions, we found it extremely difficult to get satisfactory fits to both $|S_\ell|$ and $|S_\ell|\cos(\phi_\ell-\phi_L)$ for all partial waves even by putting in several more levels. In other words, the unphysical solutions of the S-matrix elements require an unreasonable number of levels to reproduce all the cross section data. Since we did fit our S-matrix elements satisfactorily and the level parameters do reproduce the data reasonably well, we believe that the solution set selected is the correct physical one. In addition, the ^{18}F states obtained in the present work give many agreements with those obtained by Jolivette via $^{16}O(d,\alpha_1)^{14}N$ especially for the energy region where his results are most reliable (as will be discussed below).

V. DISCUSSION OF RESULTS

Figure 13 shows the isospin-mixed ^{18}F states obtained from the present work and those reported[1] from $^{16}O(d,\alpha_1)^{14}N$. States of the same spin and parity are compared separately. For each J^π, the levels from $^{16}O(d,\alpha_1)^{14}N$ are plotted on the left and those from $^{14}N(\alpha,\alpha_1)^{14}N$ on the right. We represent each level by a triangle whose base and height correspond, respectively, to the width and intensity of the state. The location of the triangle indicates its excitation energy in ^{18}F. States with large uncertainties appear as dashed triangles. The states that agree in both excitation energies and widths to within the estimated uncertainties we connect with dashed lines. Since the uncertainties are in general higher for states of lower spins, weaker intensities or larger widths, better agreements are expected for stronger or sharper resonances of spins close to L. For the same $E_x(^{18}F)$ the ^{16}O+d channel has a much higher centrifugal barrier than the ^{14}N+α channel; hence the contribution of the high spin states to the $^{16}O(d,\alpha_1)^{14}N$ cross sections is suppressed at the lower excitation energies. In our range of ^{18}F excitation, Jolivette detected no contribution of 7^- states to the $^{16}O(d,\alpha_1)^{14}N$ reaction.[1] So no comparison can be made to our 7^- states. When a higher partial wave first becomes detectable, its intensity may be too low to permit resolution of several nearby states. Hence it is not surprising that we see many more and sometimes sharper 6^+, 5^- and 4^+ states than Jolivette did. Generally speaking the agreements are quite good for 3^- states, 5^- states, and low lying 2^+ or 4^+ states. Even for the 1^- states, the comparison is better than one might expect if we consider the high uncertainties associated with $|S_1|$. As for the 6^+ states, the intensities of $|S_6|$ in $^{16}O(d,\alpha_1)^{14}N$ are so low that the comparison is hardly meaningful. We note as expected that indeed the better comparisons usually come from narrower or stronger states. The especially good agreements in 2^+ and 3^- states below 11.4 MeV are expected for two reasons. First, for both entrance channels, L is small enough that there are relatively few ambiguities in the analy-

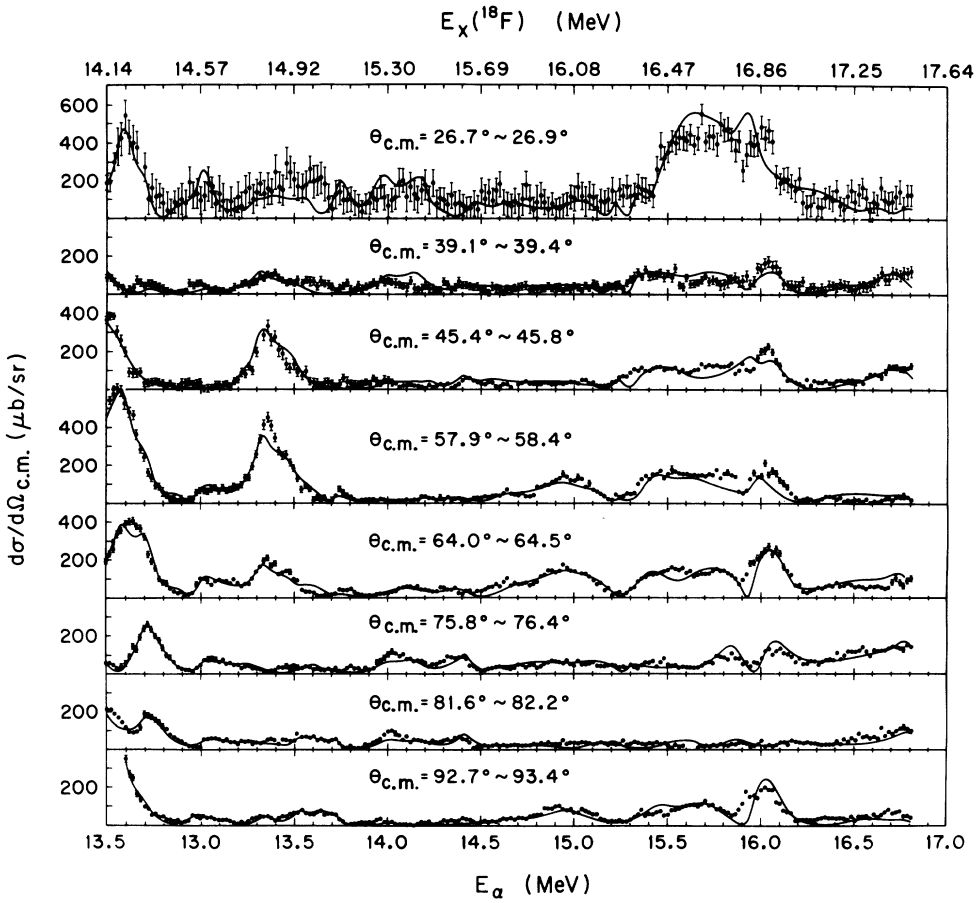

FIG. 5. The same as Fig. 1 but for different energies and angles.

sis. Second, only for this energy region, did Jolivette do the complete analysis involving a final fit of cross section data. Therefore his most reliable level parameters are for $E_x(^{18}F) <$ 11.4 MeV. The states with agreement are pointed out by the footnote, a, in Table I.

Our isospin forbidden reaction does not distinguish between a predominantly T=0 state with a small T=1 admixture, i.e., T=0(T=1) and a predominantly T=1 state with some T=0 admixture, T=1(T=0). However, the natural parity ^{18}O levels excited via $^{14}C(\alpha,\alpha_0)^{14}C$ will have T=1 analog states in ^{18}F. Therefore our ^{18}F states with the corresponding J^π and right excitation energy should be predominantly T=1 with some T=0 admixture, i.e., T=1(T=0). Morgan et al.[12] studied $^{14}C(\alpha,\alpha_0)^{14}C$ and identified the spin and parity for 13 of the levels between $9 < E_x(^{18}O) < 13$ MeV. Figure 14 shows a comparison of these states with the isospin-mixed states of ^{18}F seen in our work. The ^{18}O states with only tentative spin assignments are represented by dashed lines. For 9 of the 13 states in ^{18}O, we find a level close to the right energy for the analog state. Note that in several cases there is a clustering of isospin mixed ^{18}F states in the neighborhood of the expected analog state suggesting that the T=1 analog strength may be spread over several nearby levels. This clustering is most pronounced for the two 5^- states and lower two 4^+ states. We had hoped that the low centrifugal barrier for the present reaction would allow us to see the analog to the lowest 6^+ state in ^{18}O reported by Morgan et al. However, our lowest observable 6^+ state is still several hundred keV above the expected analog state and so is probably T=0(T=1).

Since high spin states should be narrower than low spin states, Lane and Thomas[4] predicted that with increasing excitation energy isospin conservation should reappear first for low spin states. Jolivette's S-matrix elements[1] did not confirm this prediction. In our case the results are possibly different. For each partial wave Table II shows the $|S_\ell|$'s averaged over 1 MeV intervals. For our energy range, $|\overline{S}_1|$ is flat and low. The $|\overline{S}_2|$, $|\overline{S}_3|$, $|\overline{S}_4|$ and $|\overline{S}_5|$ show tendencies to pass through regions of maximum intensities and then decrease. But $|\overline{S}_6|$ and $|\overline{S}_7|$, which only start to contribute to the reaction at much higher energies, are still on the "up" side of the trend. The general behavior for each partial wave is consistent with the Lane and Thomas discussion but may also occur for an isospin allowed reaction. In fact the approximate equality in Table II of all $|\overline{S}_\ell|$ for $E_\alpha > 13$ MeV and $\ell \leq 5$ is inconsistent with the reestablishment of isospin conservation in the low

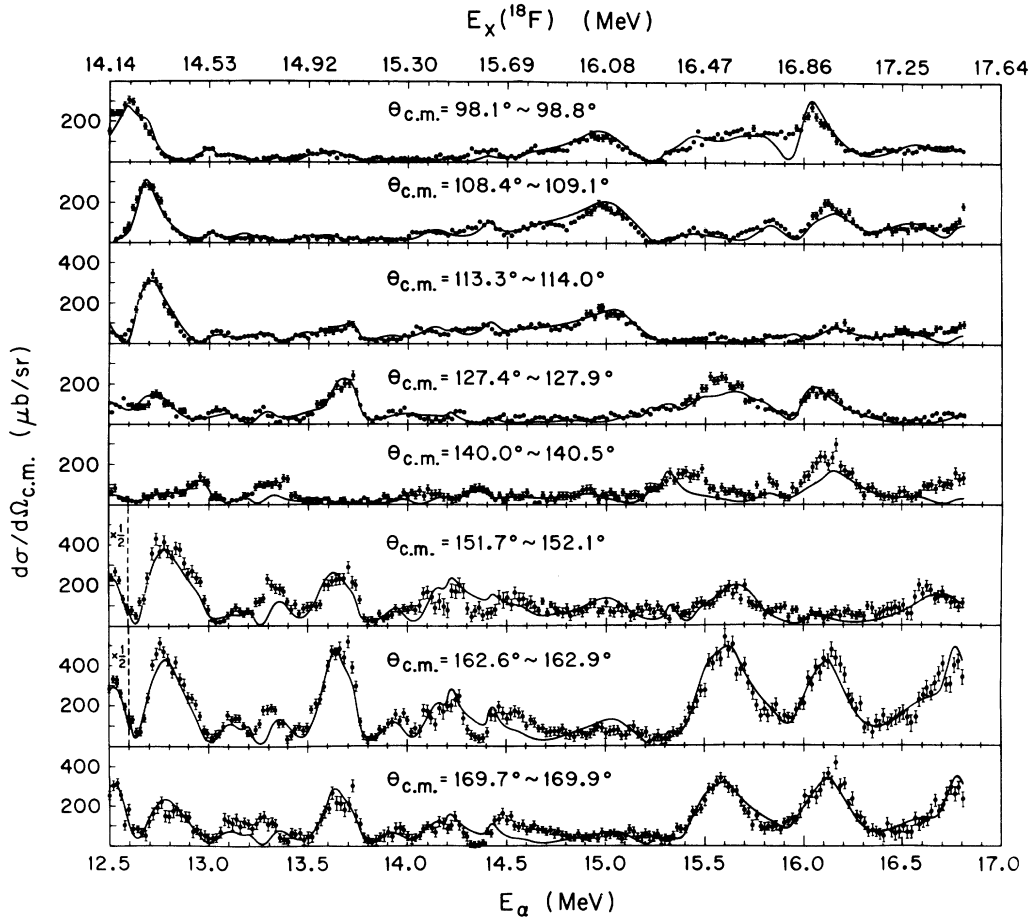

FIG. 6. The same as Fig. 1 but for different energies and angles.

partial waves. The broad and strong 1^-, T=1 giant dipole resonance around $E_x(^{18}F) \sim 20$ MeV accounts for $|\overline{S}_1|$ not approaching zero, but the failure of $|\overline{S}_2|$ and $|\overline{S}_3|$ to approach zero is harder to understand.

Jolivette[1] found from his $^{16}O(d,\alpha_1)^{14}N$ data that there was a tendency for the complex amplitudes of neighboring states with the same J^π to lie near a line through the origin and a greater tendency for several levels to add up to approximately zero total amplitude. Friedman[5] explained these results in terms of intermediate structure and bridge states, and he found that correcting for penetrability accentuates these tendencies. To provide more information on this question, we also examined the complex amplitudes of nearby ^{18}F states with same J^π. The most striking effect is found for the lowest thirteen 4^+ states as shown in Fig. 15. With very few exceptions, the states fall close to a line passing through the origin. Also, the complex amplitudes add up to nearly zero (Σ Re = .0496-.0364 = .0132; Σ Im = .0385-.0347 = .0038). No apparent correlations of similar magnitude were seen for the low lying states of other spins. The lack of correlations for the 3^- states (for which Jolivette saw strong correlations) may result from the missing (strong) states which lie below our energy region. Correction for penetrabilities should of course be made and may enhance the correlations.

VI. CONCLUSIONS

The present study of $^{14}N(\alpha,\alpha_1)^{14}N$ provides extensive new data, and the analysis introduced a new method of removing ambiguities in the partial wave analysis for $0^+ + 1^+ \leftrightarrow 0^+ + 0^+$ reaction. More reliable and new information about the structure of ^{18}F results: particularly the level parameters for 15l isospin-mixed natural parity states in ^{18}F. These level parameters reproduce the cross section measurements satisfactorily and include many of the ^{18}F states which Jolivette[1] obtained previously via $^{16}O(d,\alpha_1)^{14}N$. Some levels appear to be analogs of the ^{18}O states seen[12] in $^{14}C(\alpha,\alpha_0)^{14}C$ but in other cases the analog strength spreads over several nearby levels. The unfragmented analog states should be predominantly T=1 with some T=0 admixture.

The complex amplitudes of the lower 4^+ states fall close to a line passing through the origin

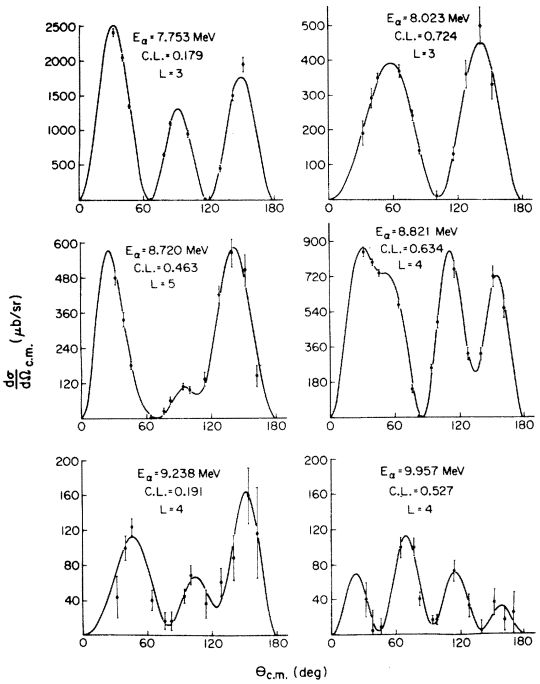

FIG. 7. Sample angular distributions for $^{14}N(\alpha,\alpha_1)^{14}N$. Error bars including the statistical errors and 2% random errors are shown whenever they exceed the point size. The curves are the fits to the data using Eq. (1). The confidence level (C.L.) indicates the goodness of the fit (.1 < C.L. < .9 is acceptable) and L is the highest partial wave used to make the fit.

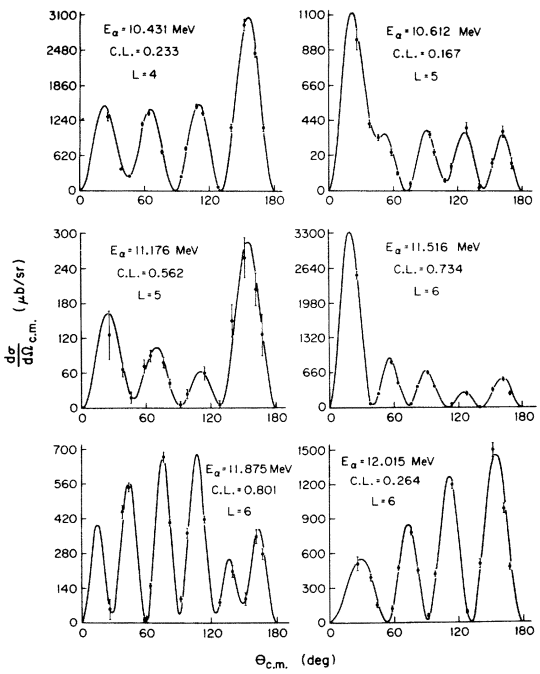

FIG. 8. The same as Fig. 7 but for different energies.

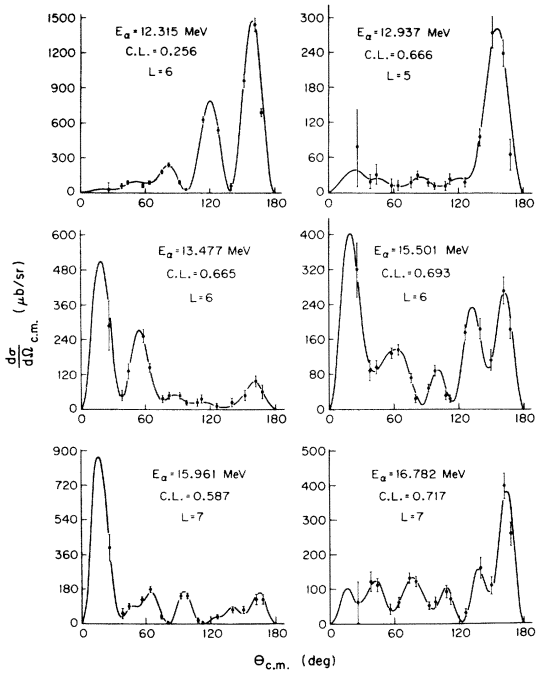

FIG. 9. The same as Fig. 7 but for different energies.

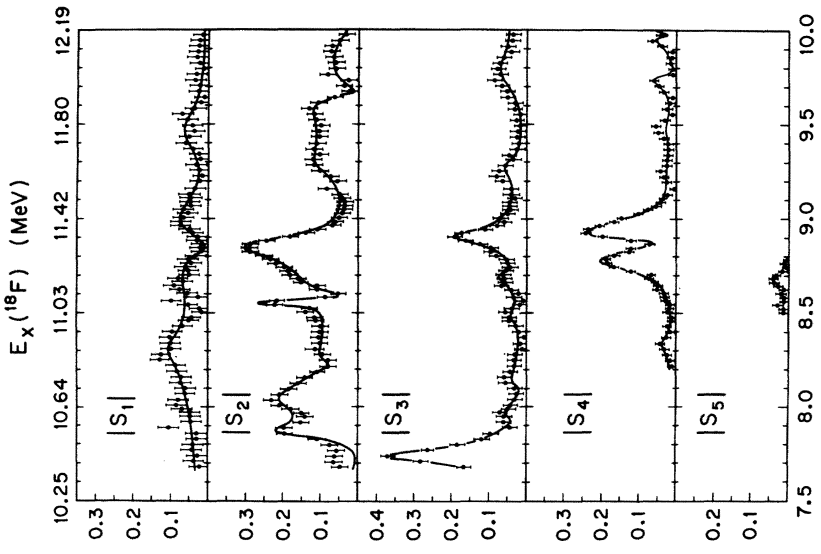

FIG. 10. Magnitudes of S-matrix elements selected as the physical solution. Averaged uncertainties obtained from the angular distribution fits are plotted for each partial wave. The solid curves correspond to the ^{18}F level parameters given in Table I.

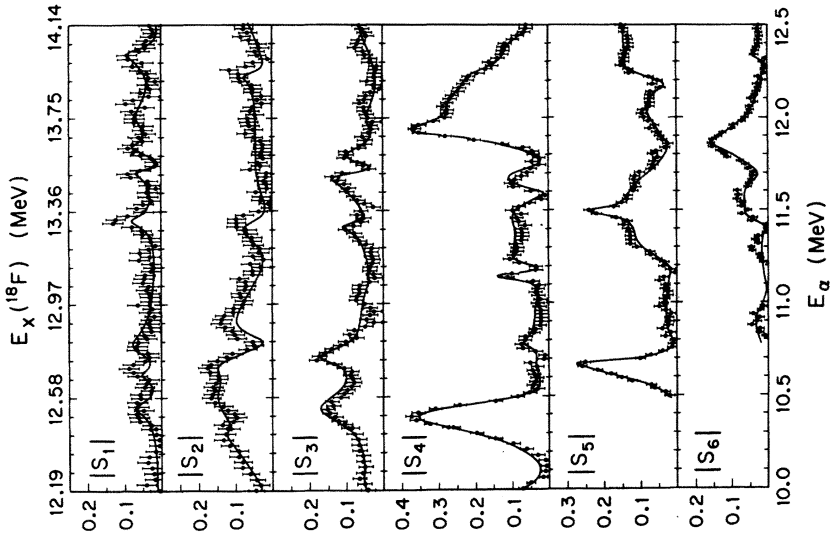

FIG. 11. The same as Fig. 10 but for different energies.

TABLE I. Isospin-mixed ^{18}F states from ^{14}N(α,α_1)^{14}N. For parameters, see Eq. (2). For comment on precision, see footnote d.

	$E_x(^{18}F)$ (MeV)	E_α (MeV)	$\Gamma_{c.m.}$ (keV)	$a_{c.m.}$ (keV)	$b_{c.m.}$ (keV)	Strength $\lvert S(E_x)\rvert$	Footnotes
			$J=1^-$				
1	10.749	8.142	535	1.7	16.4	0.062	b
2	10.886	8.319	147	-5.3	1.5	0.075	a
3	11.271	8.813	147	7.7	1.8	0.107	
4	11.431	9.019	184	6.9	-12.3	0.154	
5	11.460	9.057	313	-7.5	5.2	0.058	
6	11.789	9.470	142	4.6	1.5	0.067	a
7	12.558	10.468	45	2.1	0.3	0.093	
8	12.696	10.646	43	0.5	-0.9	0.049	
9	12.807	10.788	98	2.0	-3.5	0.082	
10	13.335	11.467	43	-2.0	0.6	0.097	c
11	13.536	11.726	19	0.4	0.9	0.101	
12	13.639	11.858	44	-0.0	2.4	0.110	a
13	13.763	12.017	120	3.1	-2.9	0.071	
14	14.028	12.358	49	0.2	2.1	0.087	a
15	14.309	12.720	75	-1.6	3.8	0.110	
16	14.719	13.247	129	5.6	5.0	0.116	a
17	14.916	13.500	79	3.0	-2.4	0.097	
18	15.073	13.702	99	1.8	-1.0	0.042	
19	15.635	14.424	101	4.5	-2.1	0.098	
20	16.160	15.099	150	1.6	-7.2	0.098	a
21	17.158	16.383	179	3.7	2.7	0.051	
			$J=2^+$				
1	10.544	7.879	43	1.9	-4.6	0.227	a
2	10.694	8.072	138	1.9	12.1	0.177	a
3	10.824	8.239	47	1.0	-0.5	0.047	a
4	11.079	8.567	23	-2.2	0.8	0.203	
5	11.111	8.608	40	3.6	-0.2	0.179	a
6	11.323	8.880	86	-1.2	-13.3	0.311	a
7	11.584	9.216	756	-67.6	-24.4	0.190	b
8	11.620	9.262	95	2.1	9.6	0.207	
9	11.924	9.653	75	1.8	4.5	0.130	a
10	12.197	10.004	252	-6.5	12.5	0.111	a
11	12.432	10.306	113	-10.2	13.2	0.295	ac
12	12.651	10.588	246	13.6	34.3	0.300	a
13	12.720	10.676	127	11.3	5.6	0.198	
14	12.869	10.868	174	19.0	-7.9	0.236	
15	13.296	11.417	73	3.3	1.2	0.097	a
16	13.424	11.582	440	13.9	-10.2	0.079	
17	13.941	12.246	46	-1.3	0.3	0.057	
18	14.287	12.691	157	-9.6	3.6	0.131	
19	14.591	13.082	51	-0.6	-0.2	0.024	
20	14.779	13.323	79	0.2	6.1	0.153	a
21	15.075	13.704	264	4.5	-2.1	0.038	
22	15.712	14.523	134	1.2	3.0	0.048	
23	16.177	15.121	195	9.7	4.5	0.110	
24	16.364	15.363	70	1.5	-3.5	0.110	
25	17.201	16.438	524	14.7	3.0	0.057	
			$J=3^-$				
1	10.448	7.755	49	-8.0	-4.8	0.381	a
2	10.599	7.949	48	-0.7	0.2	0.032	
3	10.734	8.125	37	-0.7	0.9	0.059	a
4	11.011	8.479	47	-0.4	-0.3	0.021	a
5	11.188	8.707	42	1.9	1.0	0.102	ac
6	11.354	8.921	53	0.9	-5.5	0.211	a
7	11.629	9.273	67	-2.9	-0.9	0.090	a
8	12.013	9.768	164	-7.3	-0.3	0.089	
9	12.269	10.097	69	0.3	3.5	0.102	
10	12.542	10.447	112	5.8	-7.8	0.172	a
11	12.762	10.731	58	-6.9	0.2	0.238	a
12	13.021	11.064	165	0.1	1.9	0.023	a

TABLE I (*Continued*).

$E_x(^{18}F)$ (MeV)	E_α (MeV)	$\Gamma_{c.m.}$ (keV)	$a_{c.m.}$ (keV)	$b_{c.m.}$ (keV)	Strength $\|S(E_x)\|$		Footnotes
13	13.309	11.434	35	0.8	0.9	0.069	
14	13.513	11.696	50	-2.5	2.7	0.146	
15	13.600	11.808	69	-1.9	4.6	0.142	
16	13.746	11.996	144	4.1	2.5	0.067	a
17	14.149	12.514	164	-4.4	5.7	0.087	
18	14.511	12.979	138	4.3	6.6	0.114	
19	14.696	13.217	47	1.7	-0.3	0.073	
20	14.960	13.556	71	2.1	0.1	0.059	
21	15.295	13.987	100	0.4	-4.7	0.093	
22	15.513	14.267	131	3.0	0.3	0.045	a
23	16.047	14.954	190	5.3	-2.7	0.062	
24	16.261	15.230	44	0.0	-2.3	0.107	a
25	16.865	16.006	75	-2.3	-2.0	0.082	
26	17.068	16.266	298	5.3	2.8	0.040	
27	17.380	16.667	147	-3.0	3.2	0.060	
			$J=4^+$				
1	10.910	8.349	45	-0.2	-0.6	0.025	
2	11.246	8.781	73	-4.2	-6.7	0.215	
3	11.343	8.906	56	-8.3	-1.7	0.304	ac
4	11.385	8.959	111	15.5	14.4	0.382	
5	11.570	9.198	225	4.0	-7.4	0.075	
6	11.793	9.485	67	0.4	0.5	0.019	
7	12.000	9.750	28	-0.3	-0.8	0.061	
8	12.173	9.973	22	0.8	-0.2	0.077	
9	12.203	10.011	52	-0.9	-1.9	0.081	
10	12.440	10.316	183	-15.4	-12.7	0.218	
11	12.510	10.407	94	17.1	15.6	0.496	c
12	12.565	10.477	62	-7.2	-2.7	0.248	a
13	12.702	10.653	343	11.8	7.9	0.083	
14	12.806	10.787	35	0.6	0.3	0.039	
15	13.098	11.163	25	-2.0	0.3	0.163	a
16	13.146	11.224	64	3.0	3.4	0.143	
17	13.410	11.564	110	8.3	-1.8	0.155	
18	13.518	11.702	71	0.6	-5.9	0.167	c
19	13.702	11.939	63	-10.0	-0.7	0.319	a
20	13.846	12.125	228	16.1	-20.1	0.226	
21	13.942	12.247	61	1.7	0.0	0.056	
22	14.056	12.394	54	0.7	0.1	0.025	
23	14.296	12.703	107	7.7	-0.9	0.145	
24	14.536	13.012	79	4.7	-2.8	0.140	a
25	14.703	13.226	348	-14.1	-14.0	0.114	
26	15.431	14.162	127	-6.8	-8.8	0.175	
27	15.897	14.761	471	-10.0	16.5	0.082	b
28	16.121	15.049	235	-9.3	-11.7	0.127	
29	16.327	15.313	55	-2.6	0.9	0.100	
30	16.713	15.810	180	-0.1	10.2	0.113	
31	17.245	16.494	232	-5.5	0.6	0.048	
			$J=5^-$				
1	11.187	8.705	23	-0.5	0.3	0.050	
2	12.672	10.615	80	0.6	-6.8	0.171	c
3	12.730	10.689	37	-1.6	5.4	0.306	a
4	13.186	11.275	149	0.3	-8.1	0.109	a
5	13.346	11.481	273	-23.6	22.5	0.239	
6	13.368	11.510	36	-4.0	-4.0	0.316	ac
7	13.433	11.593	149	15.3	9.7	0.244	
8	13.787	12.047	293	4.0	27.0	0.186	
9	13.931	12.234	112	8.4	6.0	0.183	
10	14.018	12.345	29	0.3	-0.2	0.021	
11	14.137	12.498	379	12.6	-23.8	0.142	a
12	14.223	12.609	110	10.8	-1.4	0.196	
13	14.372	12.801	149	-4.6	-9.1	0.136	
14	14.784	13.330	126	4.7	-4.8	0.107	

TABLE I (*Continued*).

$E_x(^{18}F)$ (MeV)	E_α (MeV)	$\Gamma_{c.m.}$ (keV)	$a_{c.m.}$ (keV)	$b_{c.m.}$ (keV)	Strength $\lvert S(E_x)\rvert$		Footnotes
15	15.015	13.628	147	-9.4	1.8	0.130	a
16	15.115	13.755	71	3.8	-0.9	0.109	
17	15.254	13.935	114	2.1	-1.3	0.043	
18	15.474	14.217	44	1.1	0.2	0.048	
19	15.647	14.440	92	-1.3	-2.1	0.054	a
20	15.762	14.587	109	0.7	-1.9	0.036	
21	16.043	14.948	151	-2.2	1.4	0.034	
22	16.417	15.430	137	-3.8	-6.6	0.110	
23	16.602	15.667	224	6.9	11.0	0.116	
24	16.873	16.016	270	-1.9	-2.7	0.024	a
25	17.224	16.468	486	-4.5	3.6	0.024	b
				$J=6^+$			
1	12.948	10.970	98	0.7	1.3	0.031	
2	13.329	11.459	62	-2.0	0.4	0.066	
3	13.489	11.665	102	1.0	2.9	0.059	
4	13.658	11.882	98	8.0	2.2	0.169	c
5	14.017	12.344	37	0.2	0.7	0.037	
6	14.139	12.501	78	0.5	-1.3	0.037	
7	14.634	13.138	104	-2.5	0.7	0.050	
8	14.893	13.471	165	3.1	4.6	0.067	a
9	15.024	13.639	82	1.9	-1.7	0.063	
10	15.634	14.422	49	-0.2	-1.2	0.049	
11	16.295	15.273	76	-1.7	-2.5	0.079	
12	16.428	15.444	183	-12.4	10.5	0.177	
13	16.637	15.713	415	28.4	14.8	0.154	
14	16.781	15.898	207	26.3	-2.1	0.255	
15	16.872	16.015	140	-15.5	-18.5	0.344	a
16	17.094	16.300	186	-0.2	1.2	0.013	
17	17.309	16.576	285	7.2	-4.7	0.061	
18	17.449	16.757	95	1.7	-1.1	0.043	
				$J=7^-$			
1	16.631	15.705	118	-0.6	-1.9	0.034	
2	16.834	15.965	73	-5.2	-0.8	0.142	
3	16.955	16.121	143	4.5	6.8	0.113	
4	17.452	16.760	109	0.4	2.7	0.051	

a. A level of the same J^π, approximate width and $E_x(^{18}F)$ occurs in $^{16}O(d,\alpha_1)^{14}N$. See also footnote d.

b. There are large uncertainties in the level parameters of this very wide level.

c. An ^{18}O state of the same J^π occurs at the corresponding $E_x(^{18}O)$. Therefore this state probably has a large T=1 amplitude.

d. While the analysis procedure gives the energy values to a keV, this precision has significance only for the relative values of nearby narrow levels. The absolute values of even the narrow levels may be in error by perhaps 10-20 keV. Uncertainties in level parameters are difficult to assess because they depend in complex ways on many factors such as the level width, the J value, the corresponding L value, the level density and the level strength. If we neglect level density and L-value effects, then the uncertainty in level width, $\Delta\Gamma$, is $\sim \sigma\Gamma/\lvert S(E_x)\rvert$ where σ is the uncertainty in $\lvert S_\ell\rvert$ as estimated from the angular distribution fits. Averaged $\bar{\sigma}_\ell$ over our energy range are $\sim$ .03 for ℓ=1; .025 for ℓ=2; .020 for ℓ=3; .016 for ℓ=4; .013 for ℓ=5; and .010 for ℓ=6 and 7. The uncertainty in E_x is approximately $\Delta\Gamma$ plus $\sim$ 20 keV systematic error. Neglect of the change in penetrability across a broad level introduces additional uncertainty. For comparison with the $^{16}O(d,\alpha_1)^{14}N$ levels, (footnote a) we estimated Jolivette's uncertainties in the same manner except for increasing his σ's by a factor 1.5.

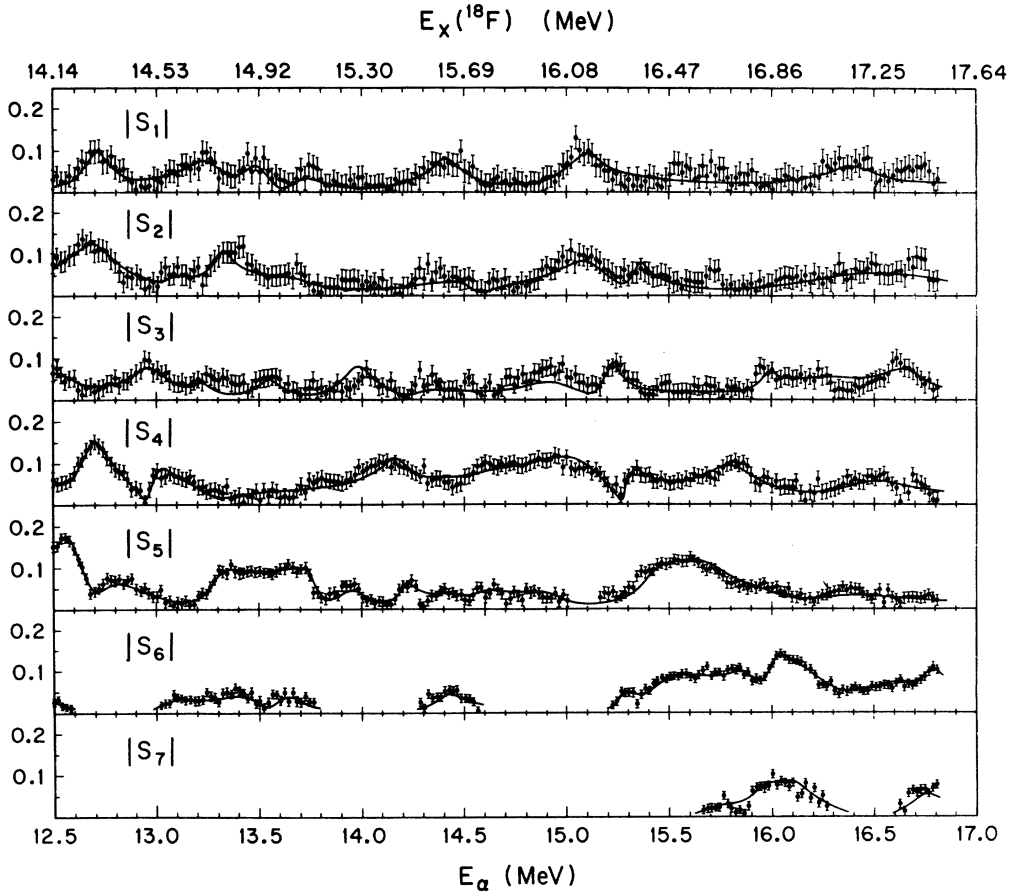

FIG. 12. The same as Fig. 10 but for different energies.

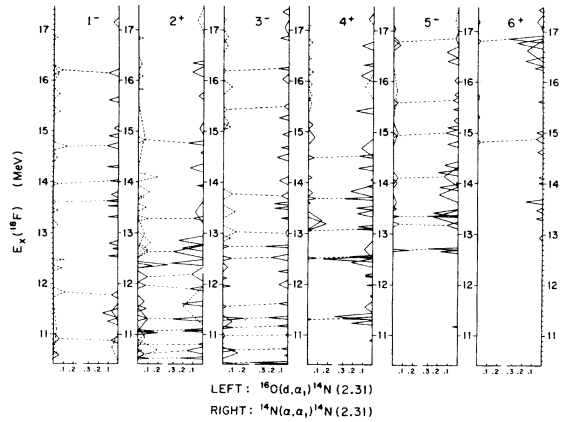

FIG. 13. Comparison of isospin-mixed ^{18}F states obtained from the present work and those seen via $^{16}O(d,\alpha_1)^{14}N$. For each J^π, the levels from $^{16}O(d,\alpha_1)^{14}N$ are plotted on the left and those from $^{14}N(\alpha,\alpha_1)^{14}N$ are plotted on the right. The base and height of each triangle correspond, respectively, to the width and intensity of the state. States with large uncertainties have dashed triangles. Dashed lines connect states that agree in both excitation energies and widths to within the estimated uncertainties.

and add up to nearly zero. Jolivette observed the same characteristics in his $^{16}O(d,\alpha_1)^{14}N$ results. Friedman[5] interprets this behavior in terms of intermediate structure and bridge states. David Wang[13] has extended Friedman's intermediate structure and bridge state analysis to our present data. Wang identified intermediate structure in all the partial waves. The bridge pairs involved appear to belong to rotational bands built on particle states of the last proton and neutron each moving in a Nilsson potential well. This work will be published separately.

ACKNOWLEDGMENTS

I sincerely thank Professor H.T. Richards for his advice and guidance throughout this work. I also thank Professor W.A. Friedman and Professor K.W. McVoy for several helpful discussions. I am grateful to Dr. P.L. Jolivette for his help in data analysis. Dr. Violeta Porto from the University of Sao Paulo, Brazil initiated the present study in 1971 with some preliminary measurements for E_α < 10 MeV. I also wish to thank Dr. J.C. Chen, Dr. H.V. Smith, Dr. B.D. Murphy, G.M. Klody, L.C. Boueres, D.J. Steck, J.H. Billen, C.A. Davis for help with accelerator operation and data taking.

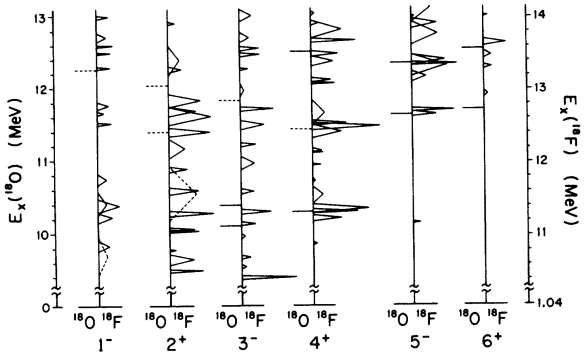

FIG. 14. Comparison of the ^{18}O states reported in Ref. 12 from $^{14}C(\alpha,\alpha_0)^{14}C$ and the ^{18}F states seen in the present work. For the significance of the ^{18}F triangles see Fig. 13 caption. Dashed lines mean uncertainty in ^{18}O spin assignments or in ^{18}F level parameters.

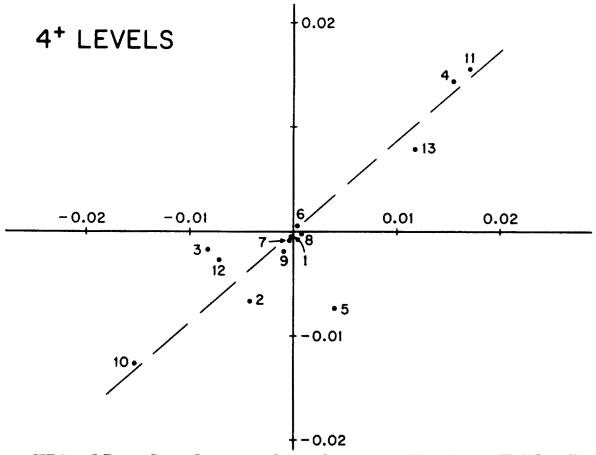

FIG. 15. Complex amplitudes a + ib from Table I for the lowest thirteen 4^+ states in ^{18}F obtained in the present work. The straight line is only a guide to the eye.

TABLE II. Energy dependence of $\overline{|S_\ell|}$

E_α range (MeV)	$\overline{\|S_1\|}$	$\overline{\|S_2\|}$	$\overline{\|S_3\|}$	$\overline{\|S_4\|}$	$\overline{\|S_5\|}$	$\overline{\|S_6\|}$	$\overline{\|S_7\|}$
7.679 - 7.989	.045	.120	.147				
8.009 - 8.987	.063	.157	.057	.070	.007		
9.007 - 9.974	.035	.075	.046	.035			
10.004 - 10.982	.040	.114	.090	.096	.040	.005	
11.002 - 11.981	.049	.048	.061	.092	.084	.052	
12.001 - 12.983	.051	.068	.046	.134	.096	.016	
13.003 - 13.984	.045	.054	.040	.044	.061	.027	
14.004 - 14.986	.034	.037	.041	.085	.031	.011	
15.006 - 15.987	.043	.047	.037	.067	.063	.060	.012
16.007 - 16.808	.047	.053	.051	.043	.033	.081	.035

† Work supported in part by the U.S. Energy Research and Development Administration.

* Present address: Computer Sciences Corporation, 8728 Colesville Road, Silver Spring, Maryland 20910.

1 P. Jolivette, Phys. Rev. C 8, 1230 (1973).

2 J. Jobst, S. Messelt and H.T. Richards, Phys. Rev. 178, 1663 (1969).

3 P.L. Jolivette and H.T. Richards, Phys. Rev. 188, 1660 (1969).

4 A.M. Lane and R.G. Thomas, Rev. Mod. Phys. 30, 257 (1957).

5 William A. Friedman, Phys. Rev. Lett. 30, 394 (1973).

6 P. Tollefsrud and P. Jolivette, Phys. Rev. C 1, 398 (1970).

7 For a brief outline of the procedure see the analysis section of this paper. More details are in the author's thesis, ref. 9. A note in preparation will include this procedure, the empirical behavior of the corresponding complex roots of the scattering amplitude, and a computer simulation which supports the empirical behavior.

8 P. Tollefsrud, Ph.D. Thesis, University of Wisconsin (1969). Available through University Microfilms, Ann Arbor, Michigan.

9 L.C. Chen, Ph.D. Thesis, University of Wisconsin (1974). Available through University Microfilms, Ann Arbor, Michigan.

10 P. Jolivette, Phys. Rev. Lett. 26, 1383 (1971).

11 A. Gersten, Nucl. Phys. B12, 537 (1969).

12 G.L. Morgan, D.R. Tilley, G.E. Mitchell, R.A. Hilko and N.R. Roberson, Nucl. Phys. A148, 480 (1970).

13 David Wang, Ph.D. Thesis, University of Wisconsin (1975). Available through University Microfilms, Ann Arbor, Michigan.